DOI: 10.1002/ejic.200900433

Synthesis of SnO_2, Fe_2O_3, and BiOCl Fibers from Inorganic Salts by a Templating Route

Rusheng Yuan,*[a] Chen Lin,[a] Baochao Wu,[a] and Xianzhi Fu[a]

Keywords: Nanostructures / Template synthesis / Solvothermal processes / Photochemistry

SnO_2, Fe_2O_3, and BiOCl fibers were synthesized from the corresponding chloride salts through a combination of templating and solvothermal processes. All the fibers possess distinct surface morphologies and lengths up to tens or hundreds of micrometers. Significantly, the BiOCl fibers with a novel heterogeneous structure were first prepared. The as-prepared BiOCl fibers exhibit good photocatalytic activity for the degradation of methyl orange in aqueous medium under UV irradiation.

Introduction

There is currently intense interest in the morphological construction of materials both at the molecular and macroscale levels because of the need for selective processing of these materials into forms suitable for applications in catalysis, separation, and other optoelectric devices. Many strategies including sol–gel,[1,2] hydrothermal or solvothermal process,[3,4] electrodeposition,[5] and templating[6,7] have been used to synthesize materials with different morphologies. Among them, the templating pathway is the most general and applicable process to realize the one-to-one transfer of the structural features from the matrix to the final product. However, in most cases for synthesis of metal oxides, metal alkoxides or other organic compounds were commonly used as the precursors. It is often necessary to add other additives to control the hydrolysis and condensation reactions. Moreover, limited alkoxides, expensiveness and toxicity to a great extent restrict the extensive applications of this method.

Alternatively, in many recent studies, many metal salts including nitrate,[8–10] acetate,[11,12] and chloride[13,14] were introduced into the template system as the precursors of the metal oxides. In our previous study,[15] a route, activated carbon fibers (ACFs) templating technique, combined with a solvothermal process has been developed to synthesize pure or composite oxide fibers with hierarchical porous structures mainly by using alkoxide precursors. Herein, we extend this strategy to construct fibrous metal oxides or oxyhalides by using pure metal chlorides as the precursors instead of organic compounds. The as-synthesized fibers exhibit large lengths up to tens or hundreds of micrometers. Furthermore, the final materials are in the macroscopic shape of textile, allowing easier manipulation than other forms such as particles, powder, and films. As for the BiOCl sample, a novel fibrous structure on the micrometer scale was first fabricated and they exhibit good photocatalytic activity for the degradation of methyl orange (MO) in aqueous medium under UV irradiation.

Results and Discussion

Figure 1 shows the SEM images of the resulting three samples. All the samples are in the macroscopic shape of textile (a typical SnO_2 photograph in the inset of Figure 1a) and consist of fibers with lengths up to tens or hundreds of micrometers. As a result of various precursors and solvents used in the solvothermal process, the as-obtained fibers present distinct surface morphologies. In the case of SnO_2, the wall of the fiber is composed of close-packed particle clusters, and several linear grooves and ridges aligned in the longitudinal direction are inherited from the ACF template. From the inset of Figure 1b, a solid crosssection is clearly observed. Different from the compact and robust structure of SnO_2 fibers, the Fe_2O_3 fibers (Figure 1c and d) are flimsy, with a crinkle-like surface resulting from shrinkage upon removal of the template. When using $BiCl_3$ as the precursor, BiOCl fibers were obtained unexpectedly instead of Bi_2O_3, and the surface morphologies depend on the temperature and solvent used. When ethanol was used as the solvent, the obtained BiOCl fibers (Figure 1e) exhibit a lava-like rough surface and solid interior structure. However, in the case of acetone as solvent at a temperature of 100 °C, the wall of the BiOCl fibers (Figure 1f) consist of lamellas assembled randomly along the length of the structure and the interior is hollow, resulting in the formation of a large plenty of

[a] Research Institute of Photocatalysis, Chemistry & Chemical Engineering College, Fuzhou University,
Fuzhou 350002, P. R. China
Fax: +86-591-83779105
E-mail: yuanrs2002@yahoo.com.cn

irregular interfaces in comparison with the solid structure. As shown in Figure 1g, the BiOCl lamellas are rectangular in shape and with a thickness of about 300 nm. More interestingly, when the solvothermal temperature was raised up to 120 °C, the BiOCl lamellas disappeared, which leads to a hollow fiber with a snowflake-like surface (Figure 1h). Therefore, the controlled synthesis of BiOCl fibers with different morphologies can be easily achieved through changing the solvent and reaction temperature.

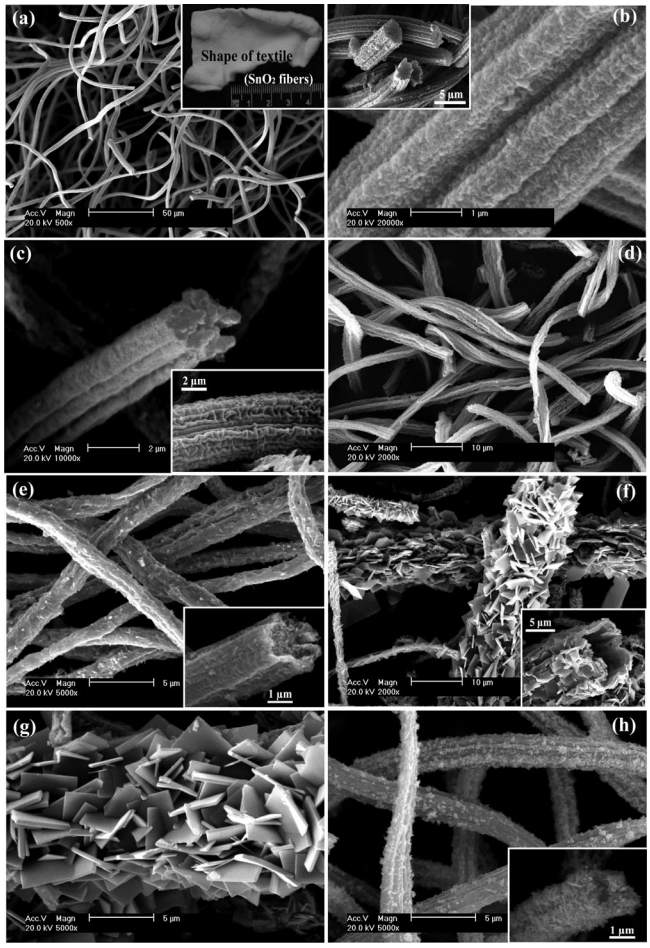

Figure 1. SEM images of the as-prepared fibers: (a, d) overview of SnO_2 and Fe_2O_3 fibers, respectively; (b, c) surface morphologies and cross sections of SnO_2 and Fe_2O_3 fibers at a high magnification; (e) BiOCl fibers prepared with ethanol solvent; (f, g, h) BiOCl fibers prepared using acetone solvent at 100 °C (f, g) and at 120 °C (h).

As shown in Figure 2, the XRD patterns of the synthesized SnO_2 and Fe_2O_3 fibers are well crystallized rutile and hematite phases, respectively. For Bi-based haloxides, full characteristic diffraction peaks of a pure phase of bismoclite appear when using ethanol solvent, whereas only several typical peaks of BiOCl occur in the case of acetone solvent. This may be attributed to the different behaviors for BiOCl crystals, as the solvent environment can strongly influence the nucleation process and epitaxial characters for certain crystal faces. In addition, the BiOCl synthesized at 100 °C presents a peak at 30° that was designated as Bi oxhydrochlorides [BiCl(OH)].[16]

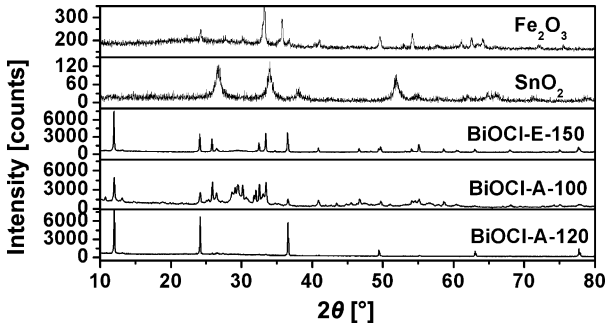

Figure 2. XRD patterns of SnO_2, Fe_2O_3, and BiOCl fibers in ethanol (BiOCl-E-150) and in acetone at 100 and 120 °C (BiOCl-A-100 and BiOCl-A-120).

The microstructures of the synthesized SnO_2, Fe_2O_3, and BiOCl fibers were further investigated by TEM, as shown in Figures 3 and 4. Figure 3a reveals that the SnO_2 fiber is composed of numerous nanoparticles with the sizes in the range from 8 to 15 nm. The inset electron diffraction pattern shows several weak Debye–Scherrer rings corresponding to the reflections of the polycrystalline tetragonal phase for rutile SnO_2. The lattice fringes in Figure 3b have an interplanar spacing of 0.334 nm belonging to the tetragonal SnO_2 crystallite, in good agreement with the XRD result. Comparatively large particles with an average size of about 20 nm are found for Fe_2O_3 samples (Figure 3c). An obvious fiber shape can also be discerned. All the indexed weak Debye–Scherrer rings (inset of Figure 3c) indicate the formation of polycrystalline hexagonal phase of Fe_2O_3. A further high-resolution TEM image (Figure 3d) of an individual crystal shows a typical crystalline domain with interplanar spacing of about 0.272 nm corresponding to the (014) plane of the hexagonal phase for hematite. Figure 4 shows the TEM images of BiOCl fibers. The interparticle pores can be observed clearly from the BiOCl fibers prepared with ethanol solvent (Figure 4a). For the BiOCl fiber synthesized with acetone at 100 °C (Figure 4c), its inner wall is full of honeycomb pores, although its outer surface is composed of many random-packed lamellas, resulting in the fiber with a heterogeneous structure. During the preparation of the sample for TEM analysis, grinding and ultrasonic dispersion resulted in breakage of the large lamellas, leaving black strips in the fiber (Figure 4c). From Figure 4d, it can be clearly seen that the lamella is almost rectangular and a highly single-crystalline tetragonal phase. Both BiOCl samples exhibit the lattice spacing of about 0.275 nm, consistent with the *d*-spacing of the (110) planes for tetragonal phase bismoclite.[17]

A possible mechanism for the formation of Fe_2O_3, SnO_2, and BiOCl fibers was proposed. ACF possesses strong adsorption and a large number of oxygen-containing functional groups (hydroxy and carboxyl) behaving as main adsorption and reaction sites, and metal ions were fixed on ACF mainly by ion exchange.[18] Because metal chlorides are very hygroscopic and easily hydrolyzable in water, the subsequent hydrolysis and condensation of metal ions will take place by the trace amounts of water in the chlorides

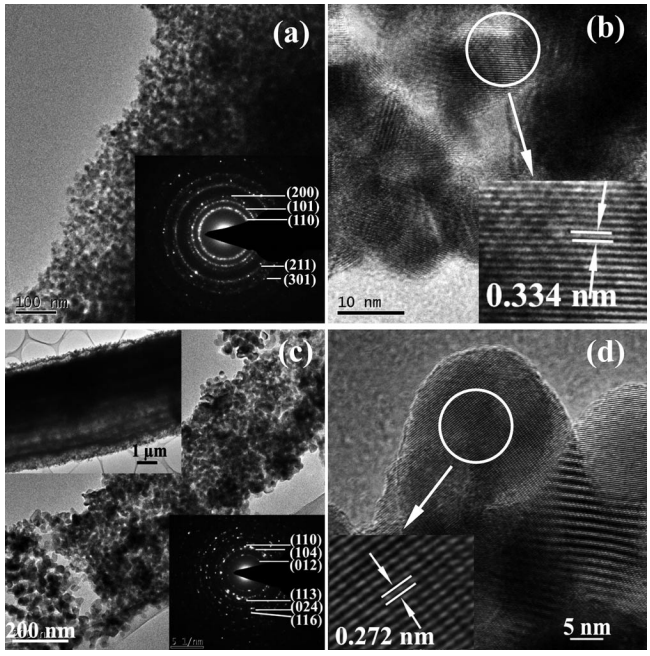

Figure 3. (a, c) TEM images of the particles of the SnO_2 and Fe_2O_3 fibers; (b, d) high-resolution TEM images of SnO_2 and Fe_2O_3 particles, respectively.

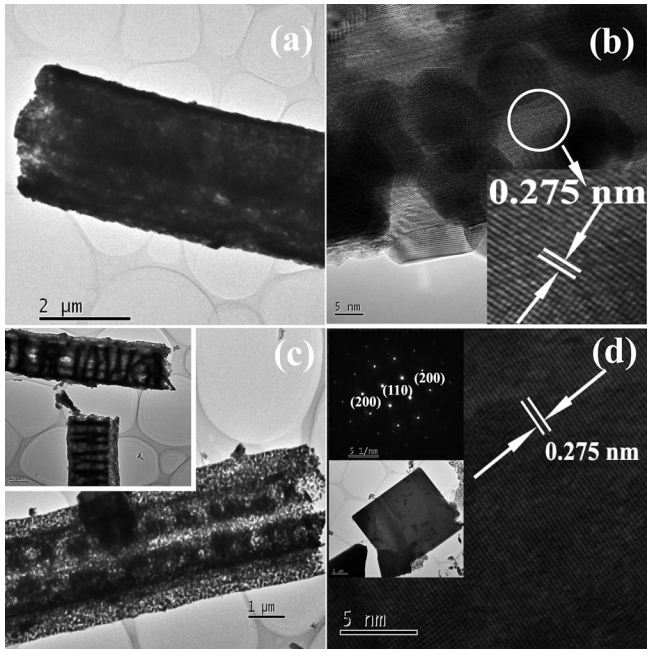

Figure 4. TEM images of (a, b) the interparticle pores and particles for the BiOCl fibers synthesized in ethanol, (c, d) the BiOCl fibers synthesized in acetone at 100 °C.

and solvent, forming a uniform coating on the pores and surface of the fibers through in situ reactions. The solid nature of the resulting fibers mainly depends on the metal ions entering into the deeper parts of the pores and the oxide framework toward thermal sintering. As for BiOCl fibers, in addition to the above-mentioned reactions, the initially obtained BiOCl nanoparticles may transform into nanoplates through a dissolution–recrystallization process,[17,19] and then they will assemble further to form larger lamellas with in-plane sizes up to several micrometers under solvothermal treatment. Different from acetone, ethanol is easy to form complexes with metal ions by using its hydroxy groups as ligands.[16] This possibly results in the Bi ions entering into the deeper parts of the pores in ethanol than the ones in acetone and formed solid fibers through thermal sintering upon calcination.

Motivated by the recent studies on BiOCl as a kind of new photocatalyst,[17,20] we investigated the photocatalysis of the as-obtained BiOCl samples to explore their potential applications. The photocatalytic degradation of MO was tested under UV irradiation after the adsorption–desorption equilibrium between BiOCl and MO was attained. A blank experiment without the photocatalyst indicates that direct photolysis of MO under the same conditions could almost be neglected. The UV/Vis spectra of MO photodegradation process are illustrated in Figure 5. For three samples, the absorption peaks belonging to MO diminish grad-

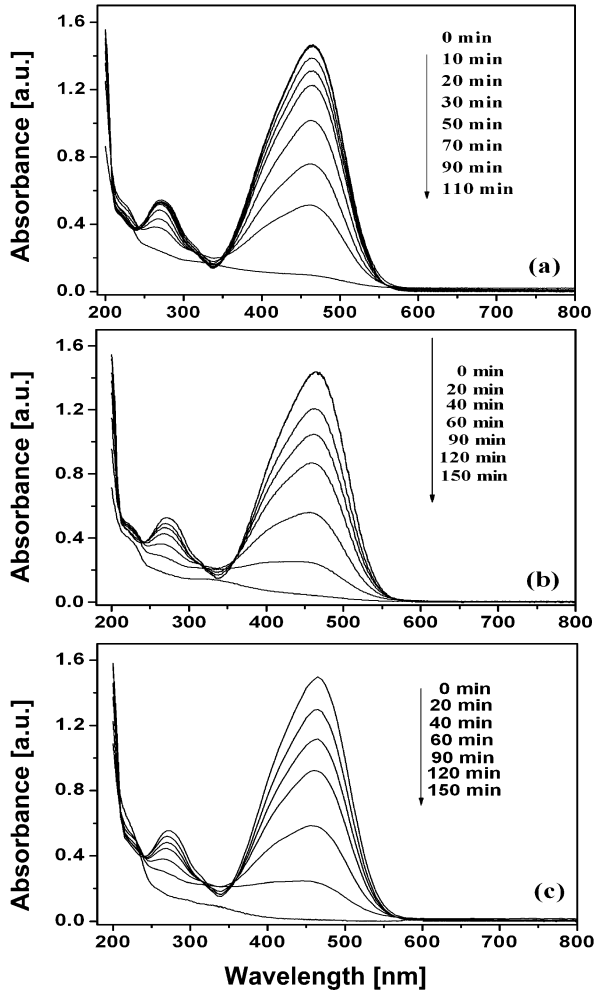

Figure 5. The UV/Vis absorption spectra of MO induced by BiOCl fibers at different irradiation times: (a) BiOCl fibers synthesized in ethanol, (b, c) BiOCl fibers synthesized in acetone at 100 and 120 °C, respectively.

ually with an increase in the irradiation time, indicating that the obtained BiOCl fibers possess photocatalytic activity for the decomposition of MO. For the BiOCl fibers synthesized with ethanol and acetone solvents, the MO dye was almost decolored after 110 and 150 min, respectively. This means that the BiOCl synthesized with ethanol solvent possesses the highest photocatalytic activity among the three samples, possibly due to the well-crystallized structure of BiOCl prepared from ethanol solvent. Meanwhile, the TOC test shows that 75% of the MO molecules were mineralized at 110 min by this sample.

Conclusions

SnO_2, Fe_2O_3, and BiOCl fibers possessing distinct morphologies were successfully synthesized through a templating route combined with solvothermal process when using the corresponding chloride salt as the precursor. The surface morphologies of BiOCl are dependent on the reaction temperature and solvent. More interestingly, a novel heterogeneous structure resulting from the in situ growth of large crystal lamellas on the thin hollow fibers was achieved for BiOCl samples. Meanwhile, the photocatalytic activities of all BiOCl samples for degradation of methyl orange indicate their potential application in water remediation in that the large sheet together with long fiber shape makes it much easier for separation from water than the form of powder.

Experimental Section

General: The ACFs used as templates has a BET surface area of 1000 $m^2 g^{-1}$ and an average pore size of about 0.78 nm. They were pretreated with concentrated nitric acid (65%) for 12 h to remove the surface impurities and create the oxygenated functionalities. After washing with distilled water, the fiber was dried at 150 °C in vacuo for 10 h. Transmission electron microscopy (TEM) and energy dispersive X-ray (EDX) spectroscopy were taken with a Philips FEI Tecnai-2000 operating at 300 KV and equipped with an EDX analyzer (Phoenix). A JEOL JSM-6700F scanning electron microscope (SEM) was used to determine the morphology of the obtained fibers. The X-ray diffraction (XRD) patterns of all samples were recorded with a Bruker D8 Advance X-ray diffractometer with Cu-K_α radiation at a scanning speed of 2° (2θ) min^{-1} in the 2θ range of 10–80°. Photocatalytic reactions were performed in a quartz tube with a total volume of 200 mL. Four 4-W UV lamps with a wavelength centered at 254 nm (Philips, TUV 4 W/G4 T5) were used as illuminating source. A sample of BiOCl (100 mg) was suspended in methyl orange (MO) aqueous solution (150 mL, δ =20 ppm) and stirred for 5 h before irradiation to ensure that adsorption/desorption equilibrium had been reached. A 3-mL aliquot was taken at the given time intervals and centrifuged (TDL-5-A) to remove the catalysts. Finally, the filtrates were analyzed with a Varian UV/Vis spectrophotometer (Cary-50). At the end of the photocatalytic reaction, the mineralization extent of MO molecules was tested with a total organic carbon (TOC) analyzer (TOC-VCPH, Shimadzu).

Preparation of the Fe_2O_3, SnO_2, and BiOCl Fibers: Typically, the acid-treated ACF (1 g) was immersed into an anhydrous ethanol solution (60 mL) containing the metal chloride (2.0 g; $FeCl_3$, $SnCl_2{\cdot}2H_2O$, and $BiCl_3$, respectively) in a Teflon-lined stainless steel autoclave. After sonication for 0.5 h to remove the air in the ACF, the autoclave was sealed and heated at 150 °C under autogenous pressure for 24 h. When it was cooled down to room temperature, the sample was taken out and rinsed with anhydrous ethanol to remove excessive metal salt, and dried at 60 °C. Finally, the composite fibers were calcined at 575 °C (ramp of 5 °C min^{-1}) in a flow of O_2 (60 mL min^{-1}) for 8 h to remove the ACF templates. BiOCl fibers were also prepared by using acetone as a solvent at 100 and 120 °C according to the same procedures.

Acknowledgments

This work was financially supported by the National Nature Science Foundation of China (No. 20701008), the Natural Science Foundation of Fujian Province of China (No. E0610011), the Key Project of Chinese Ministry of Education (No. 207053), the National Basic Research Program of China (973 Program: 2007CB613306), and the Program for Changjiang Scholars and Innovative Research Team in University (PCSIRT0818).

[1] R. Caruso, M. Antonietti, *Chem. Mater.* **2001**, *13*, 3272–3282.
[2] R. A. Caruso, *Angew. Chem. Int. Ed.* **2004**, *43*, 2746–2748.
[3] F. Gao, Q. Lu, X. Meng, S. Komarneni, *J. Mater. Sci.* **2008**, *43*, 2377–2386.
[4] H. Yang, X.-L. Wu, M.-H. Cao, Y.-G. Guo, *J. Phys. Chem. C* **2009**, *113*, 3345–3351.
[5] R. Szamocki, P. Massé, S. Ravaine, V. Ravaine, R. Hempelmann, A. Kuhn, *J. Mater. Chem.* **2009**, *19*, 409–414.
[6] Z. Lei, J. Li, Y. Ke, Y. Zhang, H. Zhang, F. Li, J. Xing, *J. Mater. Chem.* **2001**, *11*, 2930–2933.
[7] M. Tiemann, *Chem. Mater.* **2008**, *20*, 961–971.
[8] M. Sadakane, T. Horiuchi, N. Kato, C. Takahashi, W. Ueda, *Chem. Mater.* **2007**, *19*, 5779–5785.
[9] T. Valdés-Solís, G. Marbán, A. B. Fuertes, *Chem. Mater.* **2005**, *17*, 1919–1922.
[10] H. Yang, Q. Shi, B. Tian, Q. Lu, F. Gao, S. Xie, J. Fan, C. Yu, B. Tu, D. Zhao, *J. Am. Chem. Soc.* **2003**, *125*, 4724–4725.
[11] P. Huh, F. Yan, L. Li, M. Kim, R. Mosurkal, L. A. Samuelson, J. Kumar, *J. Mater. Chem.* **2008**, *18*, 637–639.
[12] H. Yan, C. F. Blanford, B. T. Holland, W. H. Smyrl, A. Stein, *Chem. Mater.* **2000**, *12*, 1134–1141.
[13] N. Shirahata, W. Shin, N. Murayama, A. Hozumi, Y. Yokogawa, T. Kameyama, Y. Masuda, K. Koumoto, *Adv. Funct. Mater.* **2004**, *14*, 580–588.
[14] J.-Y. Gong, S.-R. Guo, H.-S. Qian, W.-H. Xu, S.-H. Yu, *J. Mater. Chem.* **2009**, *19*, 1037–1042.
[15] R. Yuan, X. Fu, X. Wang, P. Liu, L. Wu, Y. Xu, X. Wang, Z. Wang, *Chem. Mater.* **2006**, *18*, 4700–4705.
[16] Z. Deng, D. Chen, B. Peng, F. Tang, *Cryst. Growth Des.* **2008**, *8*, 2995–3003.
[17] X. Zhang, Z. Ai, F. Jia, L. Zhang, *J. Phys. Chem. C* **2008**, *112*, 747–753.
[18] Z. R. Yue, W. Jiang, L. Wang, H. Toghiani, S. D. Gardner, C. U. Pittman Jr., *Carbon* **1999**, *37*, 1607–1618.
[19] J. Jiang, S.-H. Yu, W.-T. Yao, H. Ge, G.-Z. Zhang, *Chem. Mater.* **2005**, *17*, 6094–6100.
[20] K.-L. Zhang, C.-M. Liu, F.-Q. Huang, C. Zheng, W.-D. Wang, *Appl. Catal. B* **2006**, *68*, 125–129.

Received: May 12, 2009
Published Online: July 14, 2009

